Local blockage effect for wind turbines

Takafumi Nishino[1] **and Scott Draper**[2]

[1] Centre for Offshore Renewable Energy Engineering, Cranfield University, Cranfield, UK
[2] Centre for Offshore Foundation Systems, University of Western Australia, Crawley, Australia

E-mail: t.nishino@cranfield.ac.uk

Abstract. This paper presents a combined theoretical and CFD study on the fluid-mechanical limit of power extraction by a closely-spaced lateral array of wind turbines. The idea of this study originates in recent studies on the array optimisation of tidal/marine turbines, for which the power coefficient of each turbine is known to increase significantly if the lateral spacing between turbines, or the local blockage, is optimised. The present study, using 3D Reynolds-averaged Navier-Stokes (RANS) simulations of a boundary-layer flow over a closely-spaced lateral array of up to 9 actuator discs, suggests that a similar—albeit less significant—power increase due to the effect of local blockage can be achieved even for wind turbines. A possible theoretical approach to estimating this power increase is also discussed.

1. Introduction

"How to maximise the total power of a large number of turbines?" is a common question asked by both wind and tidal farm designers. From the viewpoint of a fluid dynamicist, these two problems are not identical but closely related to each other. Recent studies on the array optimisation of tidal/marine turbines [1, 2] have suggested that the best strategy to maximise the total power of a given number of turbines is to arrange them in a closely-spaced lateral array and thereby utilise the blocking effect of neighbouring turbines. For example, it has been shown theoretically by Nishino and Willden [3] that the power coefficient of a large number of turbines arrayed in the middle of an infinitely wide water channel may increase significantly from the Lanchester-Betz-Joukowsky limit of 0.593 up to another limit of 0.798 if the spacing between turbines is optimised.

A similar—albeit less significant—power increase due to such "local" or "in-field" blockage has been reported for wind turbines as well [4]; however neither the exact mechanism nor the upper limit of this power increase has been clarified yet. Hence the present study aims to explore the mechanism of such a power increase and thus clarify how significant (or not so significant) this power increase can possibly be for wind turbines. To study this systematically, a number of 3D Reynolds-averaged Navier-Stokes (RANS) simulations of an array of up to 9 turbines (represented as actuator discs) have been performed first, followed by some theoretical considerations. Although we consider a lateral array of horizontal-axis turbines for the sake of convenience, the majority of our discussion and conclusions given in this paper are equally applicable to vertical-axis turbines.

2. Blockage effect and "local" blockage effect

In this section we briefly review some of the recent theoretical models developed in the tidal energy community to understand the effect of blockage on the efficiency of ideal turbines. These models are

Content from this work may be used under the terms of the Creative Commons Attribution 3.0 licence. Any further distribution of this work must maintain attribution to the author(s) and the title of the work, journal citation and DOI.
Published under licence by IOP Publishing Ltd

essentially extended versions of the classical (Lanchester-Betz type) actuator disc momentum theory. We review the basic "single-scale" blockage effect model of Garrett and Cummins [5] first and then the "two-scale" (i.e. combined local and global) blockage effect model of Nishino and Willden [3, 6]; the latter of which is closely related to the case of wind turbines discussed later in this paper.

2.1. Blockage effect

The blockage effect model of Garrett and Cummins [5] (see also Houlsby et al. [7] and Whelan et al. [8]) considers an actuator disc placed in the middle of a uniformly confined flow passage, e.g. duct and tube. Similarly to the classical actuator disc theory, this is essentially a one-dimensional model and hence the effect of flow confinement is described solely by the blockage ratio B (the ratio of the disc area to the cross-sectional area of the flow passage); i.e. neither the cross-sectional shape of the passage nor the exact position of the turbine within the passage can be taken into account. The key difference from the classical actuator disc theory is that this model considers the conservation of energy not only for the flow going through the disc (core flow) but also for the flow "bypassing" the disc (bypass flow). The model also considers the mixing of core and bypass flows but only in the far wake region, i.e. downstream of the location where pressure equalises between the core and bypass flows; hence the entire flow is considered to become uniform again far downstream. By using this model, it is analytically shown that the upper limit of power extraction increases exponentially with the blockage ratio B. If we define the power coefficient C_P in the traditional way, i.e. based on the naturally available kinetic energy:

$$C_P = \frac{\text{Power}}{\frac{1}{2}\rho U_0^3 A} \tag{1}$$

where ρ is the fluid density, U_0 is the upstream (or undisturbed) flow speed and A is the disc area, the maximum power coefficient $C_{P\,\max}$ is shown to be $16/27 \times (1-B)^{-2}$. Note that when $B = 0$ this $C_{P\,\max}$ goes back to the Betz limit.

This theoretical model is useful, for example, when estimating the effect of wind-tunnel blockage on the output power of a turbine. However, it should be noted that this additional power due to the blockage effect essentially comes from the pressure difference induced between far upstream and far downstream of the turbine. When $B = 0$, pressure far upstream and far downstream should be the same (as assumed in the classical actuator disc theory), which means that the turbine extracts energy only from the naturally available kinetic energy and hence C_P defined in (1) is an appropriate measure of the efficiency of power extraction in this case. When $B > 0$, however, the turbine extracts energy not only from the naturally available kinetic energy but also from the pressure head induced between far upstream and far downstream of the turbine, explaining why C_P can surpass the Betz limit and even become higher than unity. In fact, this C_P can increase to infinity as B approaches to unity, in which case the power depends solely on the pressure head (as the entire flow must go through the turbine) and hence C_P defined in (1) is no longer meaningful. Clearly, this blockage effect studied by Garrett and Cummins [5] is relevant only when the entire flow passage is confined (by wind tunnel walls, for example) and cannot explain the power increase for wind turbine arrays operating outside, where there is no confinement above the turbines (and hence the overall/global blockage is zero).

2.2. Local blockage effect

The "two-scale" blockage effect model recently proposed by Nishino and Willden [3] is an extended version of the blockage effect model described above. This new model considers a large number of actuator discs arrayed laterally like a fence in the middle of a wide flow passage, thereby addressing the combined effect of "local" and "global" blockage. The original model proposed by Nishino and Willden in 2012 (hereafter referred to as NW12) assumes a complete "scale separation" between the local (device-scale) and global (array-scale) flow events including the "far-wake" mixing for each scale [3]; this assumption holds strictly and thus the model does not require any empirical or *ad-hoc* inputs when the number of discs arrayed is sufficiently large. When the number of discs is not large

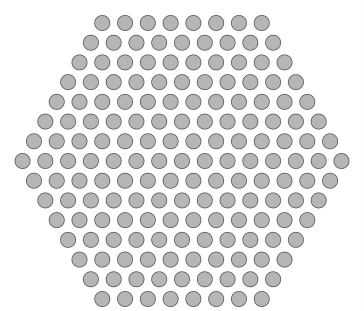


Figure 1. Schematic of a hypothetical array of a number of wind turbines (arrayed in both lateral and vertical directions) with the local blockage ratio $B_L \approx 0.4$. The NW12 model [3] suggests that this B_L is optimal and yields the theoretical upper limit, $C_{P\,\max} = 0.798$.

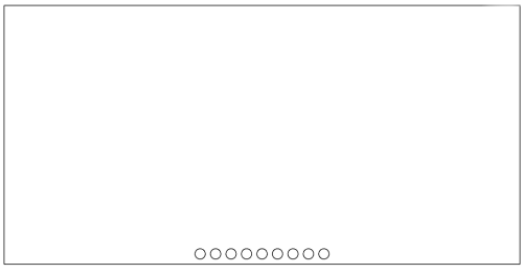


Figure 2. Cross-section of the computational domain with a lateral array of 9 actuator discs. The height and width of the domain are $25d$ and $50d$, respectively, the lateral gap between each disc is $0.5d$, and the vertical gap between the discs and the ground is also $0.5d$.

enough, however, this scale separation will not be complete and the model will need to incorporate, for example, the rate of mixing downstream of each disc empirically [6]. For the case of tidal/marine applications, i.e. discs in the middle of a wide (but shallow) water channel, recent CFD studies have suggested that the scale separation assumption employed in the NW12 model is approximately valid when the number of discs is more than 10 or so [6].

Of particular interest here, for wind energy applications, is that this two-scale model is valid even when the entire flow passage is not confined, i.e. the global blockage ratio B_G (the ratio of the total area of discs to the cross-sectional area of the entire flow passage) is zero. In this particular case, the model describes only the local blockage effect. Importantly, in this case the array of discs extracts energy only from the naturally available kinetic energy (and hence C_P defined in (1) is still a proper measure of the efficiency of power extraction) because the pressure far upstream and far downstream of the entire disc array must be the same when $B_G = 0$. It should be noted that, although the original paper by Nishino and Willden [3] considered an infinitely wide water channel as an example of the zero-global-blockage situation for tidal applications, the model itself is essentially one-dimensional and may therefore be applied to wind applications as well.[3] If we consider a hypothetical situation where a number of wind turbines are arrayed in both lateral and vertical directions, as illustrated in figure 1, these turbines (except for those near the edges of the array) would also experience the local blockage effect due to neighbouring turbines and hence, according to the NW12 model, would have the same theoretical limit $C_{P\,\max} = 0.798$ (i.e. the Nishino-Willden limit) when the local blockage B_L (the ratio of the single disc area to the cross-sectional area of each local flow passage) is about 0.4. In practice, however, wind turbines cannot usually be arrayed in the vertical direction and therefore the power increase due to the local blockage effect must be less than this hypothetical case (also, B_L can no longer be defined unambiguously). This will be discussed further in Section 4.

[3] Nishino and Willden [3] introduced the height and width of a wide water channel as well as the lateral spacing between turbines for the sake of convenience, but then showed that this two-scale blockage effect could be described solely by two independent blockage ratios; hence the model is still essentially one-dimensional [6]. Theoretically, the only key difference between the tidal application discussed in [3] and the wind application illustrated in figure 1 would be the number of turbines required to satisfy the "scale separation" assumption, since the rate of array-scale flow expansion would be different between the tidal/marine case (two-dimensional expansion) and the wind case (three-dimensional expansion). If we consider a large enough number of turbines to satisfy the scale separation assumption, these two cases are theoretically identical.

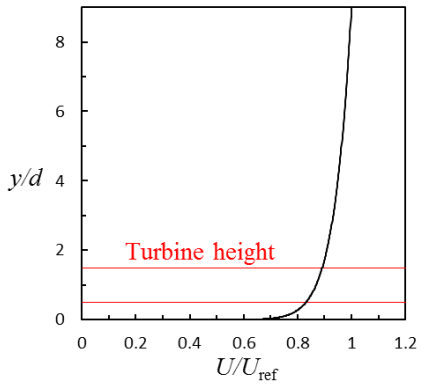


Figure 3. Streamwise velocity profile for the vertically sheared inflow case.

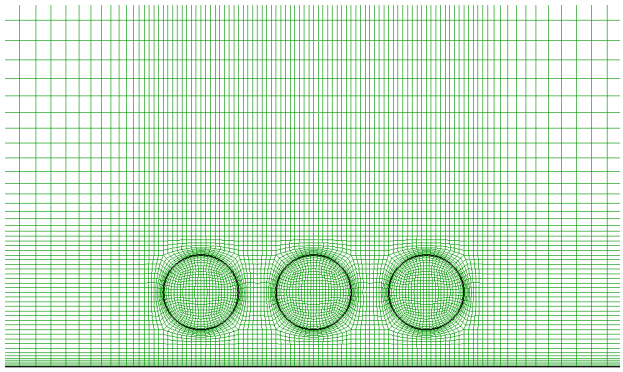


Figure 4. Cross-sectional view of the computational mesh around three actuator discs (normal resolution).

3. RANS simulations of a lateral array of wind turbines

In this section we present a series of 3D RANS simulations of a lateral array of up to 9 wind turbines (modelled as simple actuator discs without any rotations) operating near the ground, as illustrated in figure 2. Also studied is a lateral array of an infinite number of turbines, simulated using a narrower computational domain with periodic boundary conditions. Further details of the array configuration and flow conditions are described first, followed by computational methods and results.

3.1. Computational domain and array configuration

Figure 2 depicts the cross-section of our computational domain with 9 actuator discs. Except for the "infinite array" case, we employ this large computational domain of 25d height, 50d width and 100d length (where d is the disc diameter) throughout the study to ensure that the effect of global blockage is insignificant. The disc array consisting of either 1, 3, 5, 7 or 9 discs is located at the centre of the domain near the ground. The lateral gap between each disc and the vertical gap between the ground and the discs are both fixed at 0.5d. Note that the global blockage ratio B_G (which is the ratio of the total cross-sectional area of all discs to the cross-sectional area of the computational domain) slightly increases from 0.0006 to 0.006 as the number of discs increases from 1 to 9.

For the "infinite array" case, only one disc is simulated in a much narrower domain of 1.5d width (with periodic boundary conditions applied to the lateral direction). The height of the domain is the same as the other cases (25d) and therefore the global blockage ratio is still sufficiently small (B_G = 0.02) in this case. The vertical gap between the ground and the disc is again fixed at 0.5d.

3.2. Flow conditions

We consider three different inflow conditions: (i) uniform inflow with a very low level of ambient turbulence; (ii) vertically sheared inflow, i.e. boundary-layer flow; and (iii) uniform inflow with the same level of ambient turbulence as the vertically sheared inflow case. For the sake of convenience, we consider a constant air density and viscosity of 1.2kg/m^3 and 1.8×10^{-5}kg/m-s, respectively, and a disc diameter d = 100m. These, together with a reference velocity U_{ref} = 10m/s, result in the Reynolds number (based on the disc diameter) of about 67 million.

For the uniform inflow cases, uniform streamwise velocity $U = U_{\text{ref}}$ (10m/s) is applied to the inlet boundary of the domain. Inlet conditions for turbulence quantities (k and ε) will be described later in Section 3.3. Symmetry conditions are applied not only to the top and side boundaries but also to the bottom (ground) boundary of the domain; thus the uniform velocity profile is maintained throughout the domain unless the actuator discs disturb the flow.

For the vertically sheared inflow case, the mass flow through the entire computational domain is fixed such that the vertically or cross-sectionally averaged streamwise velocity $U_{\text{avg}} = U_{\text{ref}}$ (10m/s).

Symmetry conditions are again applied to the top and side boundaries, but no-slip (i.e. smooth wall) conditions are applied to the bottom (ground) boundary in this case. The streamwise velocity profile given at the inlet is shown in figure 3. This velocity profile and also the inlet profiles of turbulence quantities (not shown here) are "fully developed" profiles for the present computational domain and conditions (i.e. obtained from a preliminary simulation with periodic boundary conditions applied to the streamwise direction); hence the inlet profiles are maintained throughout the domain unless the actuator discs disturb the flow. Here the "undisturbed" streamwise velocity averaged across the disc area is U_{d0} = 8.69m/s. A summary of the flow conditions will be shown later in table 1.

3.3. Computational methods

The RANS actuator disc method used here is similar to that previously used by Nishino and Willden [6, 9] for tidal/marine applications. We solve numerically the 3D incompressible RANS equations, where the Reynolds stress terms are modelled using the standard k-ε model of Launder and Spalding [10] (with the standard wall functions applied to the bottom boundary for the sheared inflow case). Computations are performed using a commercial CFD solver ANSYS FLUENT 14 together with its user-defined function module for modifications. The solver is based on a finite volume method and is nominally second-order accurate in space. All computations are performed as steady state.

Similarly to Nishino and Willden [6, 9], each actuator disc is modelled as a stationary permeable (or porous) disc. The effect of each disc on the (Reynolds-averaged or mean) flow is considered as a loss of momentum in the streamwise (x) direction at the disc plane. The change in momentum flux (per unit area) is locally calculated as

$$M_x = K\left(\frac{1}{2}\rho U_{\mathrm{d}}^2\right) \tag{2}$$

where U_{d} is the local (rather than disc-averaged) streamwise velocity at the disc plane and K is the momentum loss factor, which is assumed to be uniform across the entire surface of all discs for each simulation. It should be noted that K = 2 is a theoretically optimal value (corresponding to the Betz limit) for an isolated disc, but for closely-arrayed discs the optimal value can be larger than 2 due to the local blockage effect; hence in this study we change the value of K between 1 and 5.

It has been shown in [9] that this RANS actuator disc method, if applied to a single disc placed in the middle of a rectangular channel with a very low level of ambient turbulence, agrees well with the analytical blockage effect model of Garrett and Cummins [5] (in terms of the power predicted for an ideal turbine). To predict the performance of real turbines, we would need a different method taking into account the aerodynamic characteristics of turbine blades (which could be modelled based on the blade element theory) and also the effect of blade-induced turbulence [11]. In this study we do not consider these issues for simplicity; however we still need to consider carefully the effect of ambient turbulence. When used with a high level of ambient turbulence, this RANS actuator disc method tends to predict strong mixing immediately downstream of the disc edges (where the shear induced by the disc is strongest) and importantly, such strong mixing in the near wake is known to increase the limit of power extraction by the disc [9, 12]. The reason for testing two different "uniform inflow" cases (with low and high levels of inlet turbulence) in addition to the "sheared inflow" case is basically to differentiate this effect (namely the near-wake-mixing effect) from the blockage effect to be studied. See table 1 for a summary of the flow conditions including the inlet conditions for k and ε.

3.4. Computational grids

Figure 4 shows a cross-sectional view of the computational mesh around three actuator discs (as an example). In this study we prepared seven different grids in total (for the cases with 1, 3, 5, 7 and 9 discs, the "infinite array" case, and the "infinite array" case with a finer resolution; see table 2 for a summary). These grids are used for both uniform inflow cases and sheared inflow cases, i.e. we use the same set of grids for different inflow conditions. As can be seen from figure 4, these grids are multi-block structured grids; we created a 2D grid first for one cross-section of the domain and then

Table 1. Summary of flow conditions.

Case	U_{avg} [m/s]	U_{d0} [m/s]	k_{in} [m^2/s^2]	ε_{in} [m^2/s^3]	$(\mu_T/\mu)_{d0}$
Uniform (low FST)	10	10	0.00015	3.02×10^{-7}	420
Vertically sheared	10	8.69	n/a	n/a	5.8×10^{5}
Uniform (high FST)	10	10	0.67335	4.18×10^{-3}	5.8×10^{5}

(FST: freestream turbulence. k_{in}: inlet value of k. ε_{in}: inlet value of ε. $(\mu_T/\mu)_{d0}$: turbulent viscosity ratio averaged across the disc area for the case without discs.)

Table 2. Summary of computational grids.

Grid	Domain width	Total number of cells
1 disc	50d	1,749,760
3 discs	50d	2,625,280
5 discs	50d	3,500,800
7 discs	50d	4,376,320
9 discs	50d	5,251,840
"infinite"	1.5d	437,760
"infinite" (F)	1.5d	3,502,080

(F: finer grid, for which the resolution was doubled in all directions.)

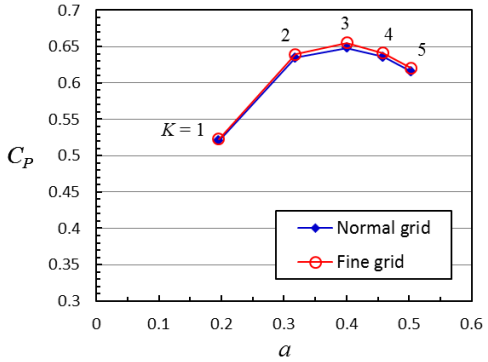


Figure 5. Effect of grid resolution on C_P (for the infinite array with low FST uniform inflow).

stacked the same 2D grid in the streamwise direction (non-equidistantly) to create a 3D grid, which consists of only hexahedral cells.

For the normal resolution grids, the minimum cell size is about 0.02d near the disc edges (in both disc-radial and disc-normal directions) and also near the bottom wall (in the wall-normal direction). For the finer resolution grid, the resolution was doubled in all directions; hence the total number of cells is 8 times larger than the normal resolution grid. As will be described in Section 3.5 the effect of grid resolution seems insignificant and therefore, unless specified, all results presented in this paper are those computed on the normal resolution grids.

3.5. Results

3.5.1. Grid sensitivity. A grid sensitivity study was performed first for the "infinite array" case with low FST uniform inflow. The results are summarised in figure 5, showing the (disc-averaged) power coefficient C_P plotted against the (disc-averaged) axial induction factor a. Note that in this study C_P and a are defined based on U_{d0} (in order to make a fair comparison between the uniform inflow and sheared inflow cases later):

$$C_P = \frac{\int M_x U_d \, \mathrm{d}A}{\frac{1}{2}\rho U_{d0}^3 A} = K \frac{\langle U_d^3 \rangle}{U_{d0}^3} \tag{3}$$

$$a = 1 - \frac{\langle U_d \rangle}{U_{d0}} \tag{4}$$

where $\langle \phi \rangle$ denotes the average of a variable ϕ over the disc area A (which can be the area of one disc or of all discs, depending on whether C_P and a are for one particular disc or for the average of all discs). It can be seen that the differences between the normal and fine resolution grids are very small for all K values tested (between 1 and 5). The difference in the maximum power coefficient $C_{P\,max}$ (obtained at $K = 3$ for this particular case) is ~1% between the two grids, suggesting that the normal resolution is sufficient.

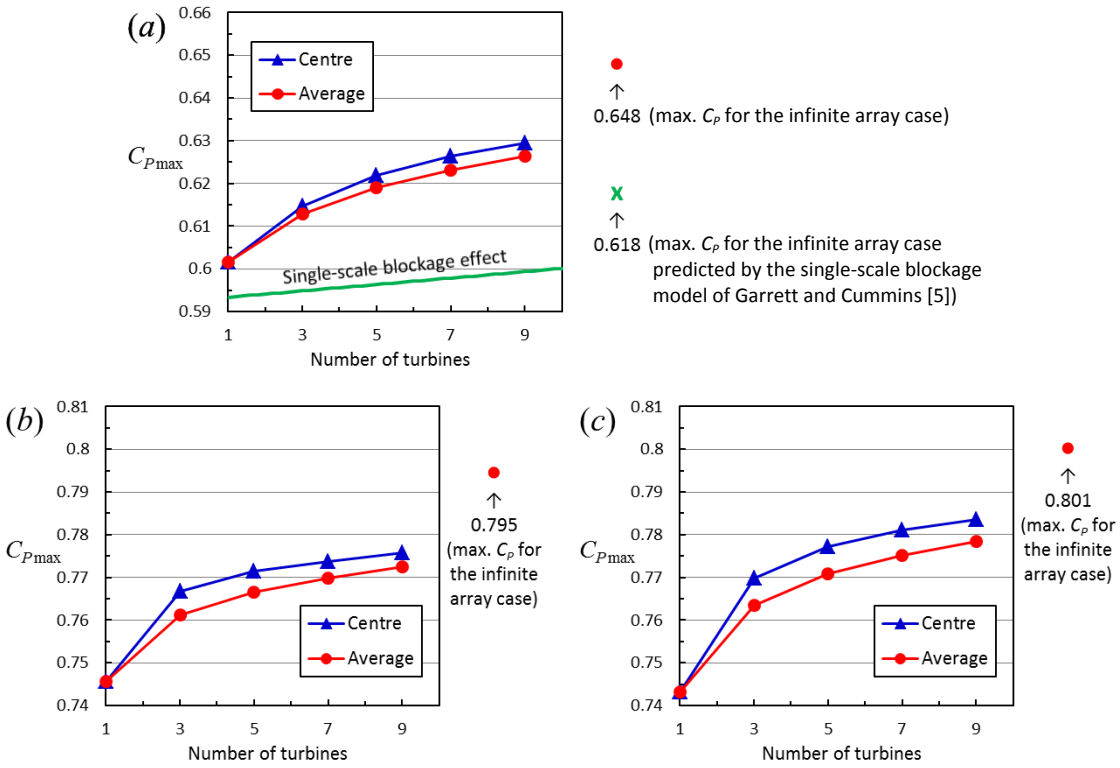


Figure 6. Effect of the number of turbines on $C_{P\,\max}$ for three different inflow conditions: (*a*) low FST uniform inflow; (*b*) vertically sheared inflow; and (*c*) high FST uniform inflow.

3.5.2. Effect of the number of turbines on $C_{P\,\max}$. Figure 6 shows the effect of the number of discs on the maximum power coefficient $C_{P\,\max}$ for the three different inflow conditions. The values of $C_{P\,\max}$ plotted here are those for the disc at the centre of the array (blue symbols) and those averaged for all discs in the array (red symbols). Also shown in figure 6(*a*) for comparison is the effect of "single-scale" blockage predicted by the theoretical model of Garrett and Cummins [5] (green line). Here the global blockage ratio B_G (varying from 0.0006 up to 0.02 as the number of discs increases from 1 to infinity) has been taken as the single-scale blockage ratio for the theoretical model.

For the case with low FST uniform inflow, the value of $C_{P\,\max}$ obtained for a single disc is 0.602, which is close to the Betz limit of 0.593 for a completely isolated disc. However, the value of $C_{P\,\max}$ increases as the number of discs increases, and importantly, the rate of increase (especially when the number of discs increases from 1 to 5 or so) is clearly higher than that predicted by the single-scale blockage effect model, indicating that this increase in $C_{P\,\max}$ is primarily due to the local blockage effect. As the number of discs increases further, the rate of increase reduces and becomes similar to that predicted by the single-scale blockage model, suggesting that about 7 to 9 discs are sufficient to take full advantage of the local blockage effect (which is about 5% increase in $C_{P\,\max}$). Note that the value of $C_{P\,\max}$ increases up to 0.648 for the "infinite array" case (corresponding to about 33 discs arrayed in the original computational domain of 50*d* width) but this additional increase in $C_{P\,\max}$ is most likely due to the slight increase in the global blockage ratio.

For the vertically sheared inflow case, the effect of the number of discs on $C_{P\,\max}$ is similar to that for the low FST uniform inflow case described above, although the values of $C_{P\,\max}$ are much higher than the previous case. The main reason of these high C_P values can be explained by comparing the results with the high FST uniform inflow case, for which the inlet values of turbulence quantities (k and ε) have been adjusted such that their values at the disc location (50*d* downstream of the inlet) are the same as those at the disc centre in the sheared inflow case. Comparing figures 6(*b*) and (*c*), it can

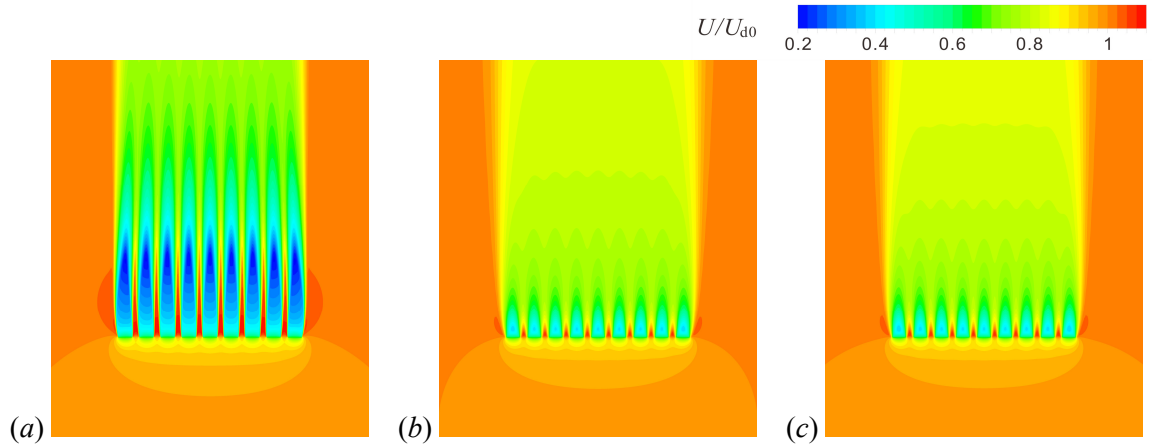


Figure 7. Streamwise velocity contours around 9 actuator discs, plotted on the horizontal plane through the disc centres: (*a*) low FST uniform inflow; (*b*) vertically sheared inflow; and (*c*) high FST uniform inflow. The axial induction factor $a = 0.37$ for all three cases.

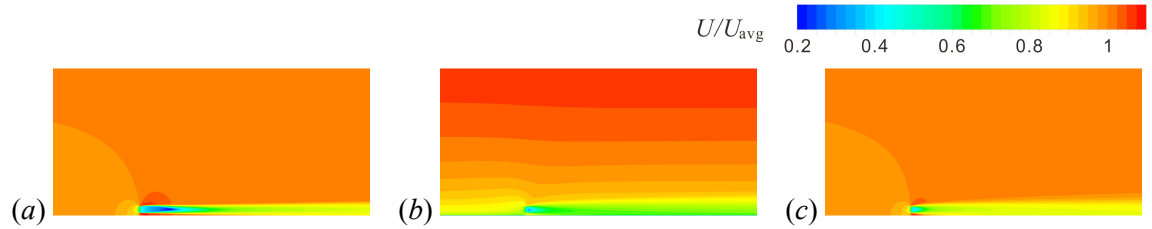


Figure 8. Streamwise velocity contours plotted on the longitudinal plane through the centre of 9 actuator discs: (*a*) low FST uniform inflow; (*b*) vertically sheared inflow; and (*c*) high FST uniform inflow. The axial induction factor $a = 0.37$ for all three cases.

be seen that the results of these two cases are very similar to each other. This suggests that the high values of $C_{P\,\max}$ for the sheared inflow case are primarily due to the high level of ambient turbulence around the discs, causing the near wake mixing effect [9] mentioned earlier in Section 3.3. It should also be noted that the increase in $C_{P\,\max}$ due to the local blockage effect in these two cases is 4~5%, which is similar to the low FST uniform inflow case. This increase is not as significant as that for the hypothetical array shown earlier in figure 1 (more than 30% increase) but is still not insignificant.

3.5.3. Two-scale flow expansion and mixing. Figures 7 and 8 show the streamwise velocity contours plotted on the horizontal and longitudinal planes, respectively, through the centre of the array of 9 actuator discs. Note that the velocity on the horizontal plane (figure 7) has been normalised by U_{d0}, whereas that on the longitudinal plane (figure 8) has been normalised by U_{avg}. Comparing the three different inflow cases, it can be seen that the level of ambient turbulence affects the prediction of the rate of mixing behind the discs significantly.

Of particular interest here is that, on the horizontal plane, we can see a clear separation of scales between the flow around each disc and the flow around the entire array (similarly to what has been discussed in [6] for tidal applications). The flow starts decelerating upstream of the entire array first due to the "array-scale" flow expansion, and then decelerates further just in front of each disc due to the "device-scale" flow expansion. Also, the wake mixing behind each disc takes place much faster than the mixing behind the entire array. This scale separation of the flow patterns (visualised on the horizontal plane) can be seen in all three different inflow cases, suggesting that the basic mechanism of the local blockage effect for wind turbines is indeed similar to that for tidal turbines.

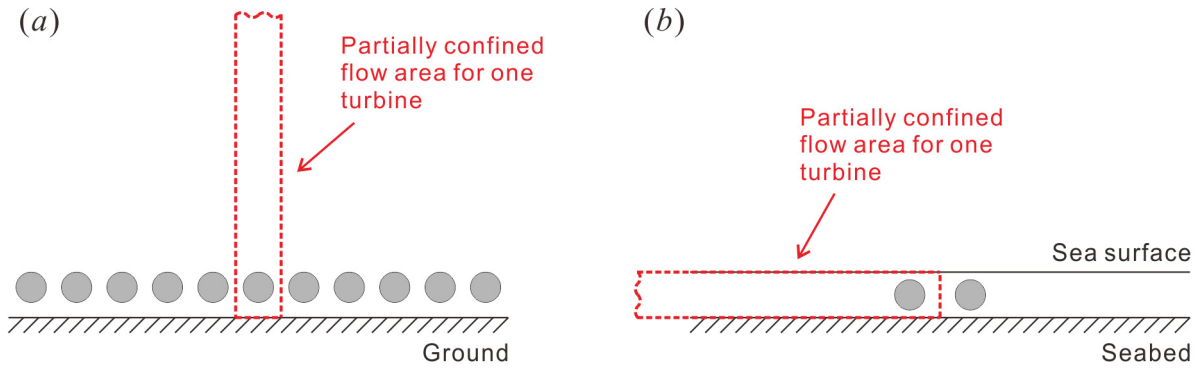


Figure 9. Configurational similarity between (*a*) an infinitely long lateral row of wind turbines and (*b*) two side-by-side tidal/marine turbines in an infinitely wide water channel.

On the longitudinal plane, it is difficult to recognise such a scale separation of the flow patterns. However, we can still see that the flow expansion and mixing takes place faster in the vicinity of the disc (where the flow is expanded/mixed three-dimensionally at the scale of the disc) compared to the regions far upstream/downstream of the disc (where the flow is expanded/mixed only vertically at the scale of the disc and only horizontally at the scale of the array).

4. Discussion and conclusions

The results of RANS actuator disc simulations have indicated that the limit of power extraction by a closely-spaced lateral array of wind turbines can be up to about 5% higher than that by the turbines placed far apart, due to the local blockage effect. This increase in power is less significant than that theoretically predicted for the hypothetical (lateral *and* vertical) array of turbines depicted earlier in figure 1, but is still potentially beneficial to wind farm developers.

It should be noted that the RANS simulations presented in this paper are only for one particular array configuration (i.e. 0.5d spacing laterally between each turbine and also vertically between the turbines and the ground), although we have tested three different inflow conditions to examine their influence on the local blockage effect. Since these computer simulations require a decent amount of computational resources, it would be desirable if this type of local blockage effect (for a lateral, but not vertical, array of turbines) can also be predicted theoretically for different configurations. If we assume that the vertical shear of the inflow is not directly related to the basic mechanism of the local blockage effect (which is a fair assumption based on the RANS results presented earlier in figure 6) and consider the "infinite array" of wind turbines with uniform inflow, the local blockage effect on these turbines should be essentially identical to that on two side-by-side tidal/marine turbines in the middle of a wide but shallow water channel with uniform inflow (note that in both cases each turbine is, effectively, locally blocked by three nearby boundaries with one open end; see figure 9). This suggests that the local blockage effect for a large number of wind turbines could be modelled in the same way as that for a (very) short array of tidal/marine turbines discussed in [6].

The difficulty here, however, is that the theoretical model of a short array of tidal/marine turbines tends to over-predict the limit of power extraction especially when the number of turbines arrayed is very small; this is essentially because the scale separation assumption does not hold for such a short array [6]. For example, if we apply this short tidal array model (with $n = 2$, where n is the number of turbines) to the low FST uniform inflow case of "infinite array" of wind turbines, the model predicts $C_{P\,\max} = 0.71$, which is substantially higher than the corresponding RANS actuator disc prediction of $C_{P\,\max} = 0.65$ shown earlier in figure 6(*a*). As discussed in [6], what we need to know here (in order to correct the theoretical model for such a short array of tidal/marine turbines) are essentially the rates of "device-scale" flow expansion and mixing relative to the rates of "array-scale" flow expansion and mixing. From the viewpoint of an infinitely long lateral row of wind turbines, this may be rephrased as

follows: we need to know the rates of three-dimensional flow expansion and mixing (taking place in the vicinity of each turbine) relative to the rates of vertical flow expansion and mixing (taking place more upstream and downstream of the row of turbines).

In conclusion, the basic mechanism of the local blockage effect for wind turbines seems closely related to that for tidal/marine turbines. The concept of two-scale flow modelling recently proposed for tidal/marine turbines seems useful to understand the local blockage effect for wind turbines as well. Further communications between wind energy researchers and tidal/marine energy researchers would be beneficial to both research areas.

References

[1] Draper S and Nishino T 2014 Centred and staggered arrangements of tidal turbines *J. Fluid Mech.* **739** 72-93
[2] Hunter W, Nishino T and Willden R H J 2015 Investigation of tidal turbine array tuning using 3D Reynolds-averaged Navier-Stokes simulations *Int. J. Marine Energy* **10** 39-51
[3] Nishino T and Willden R H J 2012 The efficiency of an array of tidal turbines partially blocking a wide channel *J. Fluid Mech.* **708** 596-606
[4] McTavish S, Rodrigue S, Feszty D and Nitzsche F 2014 An investigation of in-field blockage effects in closely spaced lateral wind farm configurations *Wind Energy* (published online)
[5] Garrett C and Cummins P 2007 The efficiency of a turbine in a tidal channel *J. Fluid Mech.* **588** 243-51
[6] Nishino T and Willden R H J 2013 Two-scale dynamics of flow past a partial cross-stream array of tidal turbines *J. Fluid Mech.* **730** 220-44
[7] Houlsby G T, Draper S and Oldfield M L G 2008 Application of linear momentum actuator disc theory to open channel flow *Tech. Rep.* OUEL 2296/08 University of Oxford
[8] Whelan J I, Graham J M R and Peiró J 2009 A free-surface and blockage correction for tidal turbines *J. Fluid Mech.* **624** 281-91
[9] Nishino T and Willden R H J 2012 Effects of 3-D channel blockage and turbulent wake mixing on the limit of power extraction by tidal turbines *Int J. Heat Fluid Flow* **37** 123-35
[10] Launder B E and Spalding D B 1974 The numerical computation of turbulent flows *Comput. Methods Appl. Mech. Eng.* **3** 269-89
[11] Nishino T and Willden R H J 2014 Low-order modelling of blade-induced turbulence for RANS actuator disk computations of wind and tidal turbines *Wind Energy - Impact of Turbulence (Research Topics in Wind Energy* vol 2*)* eds M Hölling, J Peinke and S Ivanell (Berlin: Springer) pp 153-58
[12] Nishino T and Willden R H J 2013 The efficiency of tidal fences: a brief review and further discussion on the effect of wake mixing *Proc. ASME 32nd Int. Conf. on Ocean, Offshore and Arctic Engineering (Nantes)* OMAE2013-10207



https://dspace.org/

Local blockage effect for wind turbines

Nishino, Takafumi; Draper, Scott

2015-06-11
IOP Publishing
https://DOI.org/10.1088/1742-6596/625/1/012010
Nishino T, Draper S. (2015) Local blockage effect for wind turbines. In: Journal of Physics: Conference Series, Volume 625, Wake Conference 2015, 9-11 June 2015, Visby, Sweden, Article number 012010

Downloaded from a DSpace repository. https://dspace.org/